Associative Charge Transfer Reactions. Temperature Effects and Mechanism of the Gas-Phase Polymerization of Propene Initiated by a Benzene Radical Cation†

Yehia Ibrahim, Michael Meot-Ner Mautner,* and M. Samy El-Shall*

Department of Chemistry, Virginia Commonwealth University, Richmond, Virginia 23284-2006

Received: December 31, 2005; In Final Form: March 1, 2006

In associative charge transfer (ACT) reactions, a core ion activates ligand molecules by partial charge transfer. The activated ligand polymerizes, and the product oligomer takes up the full charge from the core ion. In the present system, benzene$^{+\bullet}$ ($Bz^{+\bullet}$) reacts with two propene (Pr) molecules to form a covalently bonded ion, $C_6H_6^{+\bullet} + 2\ C_3H_6 \rightarrow C_6H_{12}^{+\bullet} + C_6H_6$. The ACT reaction is activated by a partial charge transfer from $Bz^{+\bullet}$ to Pr in the complex, and driven to completion by the formation of a covalent bond in the polymerized product. An alternative channel forms a stable association product $(Bz{\cdot}Pr)^{+\bullet}$, with an ACT/association product ratio of 60:40% that is independent of pressure and temperature. In contrast to the $Bz^{+\bullet}$/propene system, ACT polymerization is not observed in the $Bz^{+\bullet}$/ethylene (Et) system since charge transfer in the $Bz^{+\bullet}$(Et) complex is inefficient to activate the reaction. The roles of charge transfer in these complexes are verified by ab initio calculations. The overall reaction of $Bz^{+\bullet}$ with Pr follows second-order kinetics with a rate constant of k (304 K) $= 2.1 \times 10^{-12}$ cm^3 s^{-1} and a negative temperature coefficient of $k = aT^{-5.9}$ (or an activation energy of −3 kcal/mol). The kinetic behavior is similar to sterically hindered reactions and suggests a [$Bz^{+\bullet}$(Pr)]* activated complex that proceeds to products through a low-entropy transition state. The temperature dependence shows that ACT reactions can reach a unit collision efficiency below 100 K, suggesting that ACT can initiate polymerization in cold astrochemical environments.

I. Introduction

We recently reported a novel class of ion−molecule reactions that are charge-transfer driven by the formation of covalent bonds.[1,2] In these reactions, gas-phase molecules form a cluster around a core ion that activates the ligand molecules by partial charge transfer. The activated molecules dimerize with covalent bond formation, whose exothermicity drives the reaction. The dimerized product has low ionization energy (IE) and takes up the full charge from the core ion. These processes may be called associative charge transfer (ACT) reactions. Analogous processes in protonated systems lead to the formation of hydrogen bonds in associative proton transfer (APT) reactions.[3−6]

These systems may require a sufficiently large cluster to make the reactions energetically feasible. Such size-specific reactions have been studied in preformed clusters generated by supersonic beam expansions.[7−12] However, in our reaction systems, clusters need to be assembled stepwise until a sufficiently large cluster is formed to allow the reaction to take place. The rate of the overall reaction may be then affected by the kinetics of both the cluster formation and the intracluster reaction.

The buildup of the clusters is facilitated at low temperatures, and the rates of the overall ACT or APT reactions can increase with decreasing temperature. In fact, we recently observed an APT reaction with an unprecedented large negative temperature coefficient.[5,6] In that reaction, the proton transfer from $C_6H_6^{+\bullet}$ to four or more H_2O molecules forms hydrogen-bonded water clusters $(H_2O)_nH^+$ with a temperature coefficient of $k = aT^{-67} \pm 4$ (or an activation energy of −34 kcal/mol).

Because of the basic similarity of the ACT and APT mechanisms, it is of interest whether ACT reactions also have negative temperature coefficients. We studied ACT reactions in the toluene$^{+\bullet}$/isobutene and benzene$^{+\bullet}$/propene systems.[1,2] In these reactions, the charge is transferred from the ionized aromatic to two olefin molecules that condense to form a covalently bonded dimer ion, as shown in reaction 1 for the benzene$^{+\bullet}$/propene system.

$$C_6H_6^{+\bullet} + 2\ C_3H_6 \rightarrow C_6H_{12}^{+\bullet} + C_6H_6 \qquad (1)$$

In this system, the charge transfer from $C_6H_6^{+\bullet}$ to a single C_3H_6 molecule would be endothermic by 11.2 kcal/mol, but the overall reaction with two C_3H_6 molecules to form a covalent product such as 3-hexene$^{+\bullet}$ is exothermic by 30 ± 1 kcal/mol.[13] Therefore, the formation of a dimer ion makes the overall process of charge transfer and covalent condensation significantly exothermic.

The mechanism of these new reactions and their dependence on temperature and pressure are of fundamental interest and are also relevant to their possible roles in gas-phase polymerization and in astrochemistry. For example, applications of these reactions in developing novel initiation methods for the gas-phase polymerization of olefin monomers could provide significant contributions not only to basic polymer science, but also to technological applications such as the synthesis of defect-free, uniform thin polymeric films with advanced properties.[14] Also, the role of charge transfer from ionized aromatics in the formation and growth of large hydrocarbon ions at lower temperatures is relevant to many astrochemical processes in interstellar medium.[15]

In our previous studies of ACT reactions, selective ionization of the aromatic component was necessary to avoid direct ionization of the olefin monomer. For this reason, we used resonant two-photon ionization coupled with high-pressure mass spectrometry (R2PI−HPMS) in which the aromatic component

† Part of the "Chava Lifshitz Memorial Issue".

* Corresponding authors. E-mail: selshall@hsc.vcu.edu (M.S.E.-S.), m.mautner@eco88.com (M.M.-N.M.).

10.1021/jp057595a CCC: $33.50
Published on Web 04/25/2006

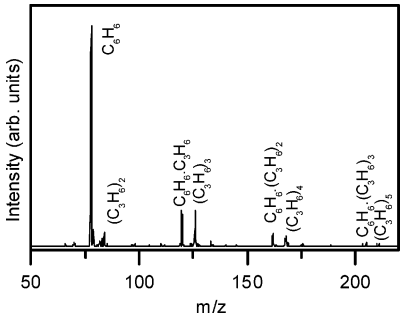

Figure 1. Mass spectrum obtained following the injection of $C_6H_6^{+\bullet}$ into a mixture of propene (15 mTorr) in He (2090 mTorr) at 302 K.

was ionized selectively. In the present work, we employ the mass-selected ion mobility technique in which the benzene radical cation is generated separately and then injected into a mixture containing only the olefin molecules and a third-body inert gas without the neutral aromatic molecules. This would allow for the temperature and pressure studies of reaction 1 and avoid possible kinetic and mechanistic complications due to the formation of the benzene dimer cation. We also provide a theoretical study of the structures and energetics of the species involved in the ACT process.

II. Experimental and Computational Methods

The experiments were conducted using the Virginia Commonwealth University (VCU) ion mobility mass spectrometer that was described previously.[16,17] The mobility cell was heated by cartridges or cooled by liquid nitrogen. The temperature was monitored at several locations in the cell to ensure thermal homogeneity. Benzene ions $C_6H_6^{+\bullet}$ (i.e., $Bz^{+\bullet}$) were formed by electron impact, mass selected, and injected into a mixture of propene in He carrier gas in the mobility cell. After transiting the mobility cell, the ions exited through a pinhole and were detected by a quadrupole mass spectrometer. The injection was pulsed and peaks of arrival time distributions (ATDs) were collected, with the peak areas representing the intensities of the ions.

The structures of the $C_6H_6^{+\bullet}(C_3H_6)_{1,2}$ and $C_6H_6^{+\bullet}(C_2H_4)$ cations were optimized at the ROHF/6-31+G(d,p) level of theory using the Gaussian 03 (G03) software package.[18] The optimization was verified by calculating the vibrational frequencies. The binding energies were calculated using MP2 energies on the optimized ROHF/6-31+G(d,p) structures and corrected for the zero-point energies (ZPEs) and the basis-set superposition error (BSSE). The BSSE was calculated using the counterpoise method, as implemented in the G03 software. The charge on each component within each cluster was calculated by adding all atomic Mulliken charges.

III. Results and Discussion

1. ATDs. Figure 1 displays a typical mass spectrum obtained following the injection of $C_6H_6^{+\bullet}$ into a propene/He mixture in the mobility cell. As expected, both the adduct channel $C_6H_6^{+\bullet}$-$(C_3H_6)_n$ and the condensation channel $(C_3H_6)_n^{+\bullet}$ are observed. At higher concentrations of propene (propene number density $N[C_3H_6] > 10^{14}$ molecules/cm^3), the $(C_3H_6)_n^{+\bullet}$ ions with $n = 2-6$ become the major products, while the $C_6H_6^{+\bullet}(C_3H_6)_n$ ions with $n = 1-3$ are the minor products.

Figure 2 displays the ATDs of the ions in the $Bz^{+\bullet}$/Pr ($Bz^{+\bullet}$/C_3H_6) system. The graph is divided into two parts showing the $Bz^{+\bullet}(Pr)_n$ adducts and $Pr_n^{+\bullet}$ polymerization products. The smallest ions $C_6H_6^{+\bullet}$ and $(C_3H_6)_2^{+\bullet}$ with the highest mobilities

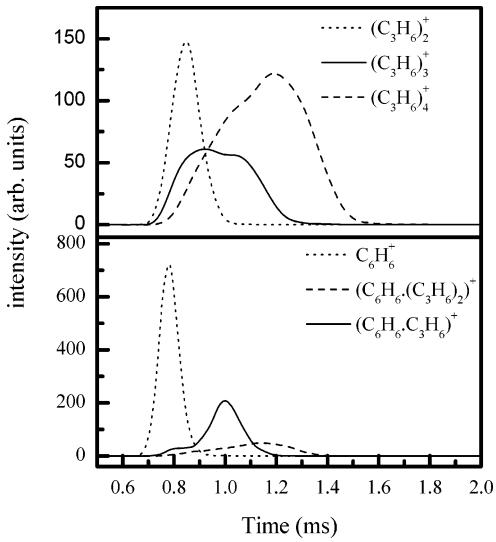

Figure 2. ATDs of ions observed following the injection of $C_6H_6^{+\bullet}$ into a mixture of 58 mTorr of propene in 2.05 Torr of He at $T = 301$ K and injection energy = 15 eV (lab.).

SCHEME 1

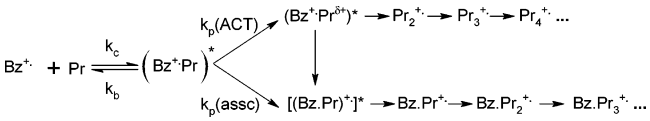

arrive first in the two groups, respectively. The ATD peak shapes of the higher adducts in both groups are skewed to longer times, characteristic of large slower product ions that build up in the cell as the reactant ion moves along the cell and arrives at the exit hole after the faster reactant ions. Importantly, the ATD peaks of the adducts $Bz^{+\bullet}(Pr)_n$ do not overlap with the ATD peak of the $Bz^{+\bullet}$. This indicates that the adducts are not in association equilibrium with $Bz^{+\bullet}$, but rather the association is irreversible under these conditions. The irreversible adducts may be covalently bonded propylbenzene ions, or noncovalent clusters.

2. Pressure and Temperature Effects on the Rate Coefficients. In the experiments, we observe the disappearance of the injected $Bz^{+\bullet}$ ion and the formation of two primary products $Pr_2^{+\bullet}$ and $Bz{\cdot}Pr^{+\bullet}$ in parallel. Further Pr molecules add subsequently to each of the primary products.

First-order rate constants for the reaction of the injected $Bz^{+\bullet}$ ions into both channels were measured by varying the ion residence times and using the relation $\ln([Bz^{+\bullet}]_t/[Bz^{+\bullet}]_o) = -k_1 t$ where the term on the left-hand side is calculated from the intensity of the $Bz^{+\bullet}$ reactant ion as a fraction of the total ion intensity, that is, $[Bz^{+\bullet}]_t/[Bz^{+\bullet}]_o = [Bz^{+\bullet}]/([Bz^{+\bullet}] + \Sigma[\text{Products}]^{+\bullet})$. Here, k_1 is the pseudo-first-order rate coefficient of Scheme 1, and the second-order rate coefficient k_2 is calculated from $k_1 = k_2[N(\text{Pr})]$, where N(Pr) is the number density (molecules/cm^3) of propene in the mobility cell. Rate coefficients for each of the competitive channels were calculated using the normalized ion intensities of the products, k_1 (ACT) $= k_1 I(Pr)_2^{+\bullet}/[I(Pr)_2^{+\bullet} + I(Bz{\cdot}Pr)^{+\bullet}]$, and k_1 (association) $= k_1$-$(Bz{\cdot}Pr)^{+\bullet}/[I(Pr)_2^{+\bullet} + I(Bz{\cdot}Pr)^{+\bullet}]$. The intensities of the consecutive higher adducts of each channel were added to the respective primary ions.

The results of the pressure studies are shown in Table 1. The pressure of the He bath gas could be varied only between 1.0 and 1.9 Torr, with only a slight increase in k_2, within experimental error. Effects of the partial pressure of propene

TABLE 1: Pressure Effects on the Rate Coefficient of the Reaction of Benzene$^{+\bullet}$ with Propene and on the Product Distribution, in Terms of the Fraction of Reaction into the Propene Dimer Channel

Effect of the bath gas *P*(He), at constant *P*(Propene) = 10 mTorr, at *T* = 274 K

P_{total} (mTorr)	k_2 (cm^3 s^{-1})[a]	fraction ACT
1004	1.7×10^{-12}	0.47
1320	1.4×10^{-12}	0.52
1606	1.8×10^{-12}	0.58
1905	2.0×10^{-12}	0.58

Effect of the propene partial pressure *P*(propene) at constant total pressure *P*(propene) + *P*(He) = 1091 mTorr, at *T* = 271 K

$P_{propene}$ (mTorr)	k_2 (cm^3 s^{-1})[a]	fraction ACT
10	2.0×10^{-12}	0.58
21	2.2×10^{-12}	0.66
30	2.4×10^{-12}	0.69
40	2.3×10^{-12}	0.63
50	2.6×10^{-12}	0.72

Effect of the propene partial pressure *P*(propene) at constant *P*(propene + He) = 1700 mTorr, at *T* = 245 K

$P_{propene}$ (mTorr)	k_2 (cm^3 s^{-1})[a]	fraction ACT
4	4.7×10^{-12}	0.52
9	4.0×10^{-12}	0.60
20	4.5×10^{-12}	0.68
30	4.3×10^{-12}	0.66

[a] Second-order rate coefficient with respect to propene, calculated from the measured pseudo-first-order rate coefficient using $k_2 = k_1/[N(\text{propene})]$.

TABLE 2: Temperature Effects on the Rate Coefficients for the Total Reaction, and for Reactions into the ACT Channel to Form $C_6H_{12}^{+\bullet}$ and into the Association Channel to Form the $C_6H_6^{+\bullet}\cdot C_3H_6$ Adducts

T (K)	k_2 (total)[a]	k_2 (ACT)[a]	k_2 (assoc)[a]	fraction ACT
372	0.3	0.1	0.2	0.34
352	0.4	0.2	0.2	0.47
323	0.5	0.4	0.2	0.68
306	1.0	0.7	0.4	0.64
304	1.4	1.0	0.4	0.71
271	2.4	1.6	0.8	0.66
245	4.3	2.8	1.5	0.66
234	4.6	2.7	1.9	0.58
215	7.9	4.8	3.1	0.60
215	8.9	5.4	3.5	0.62
195	16.2	10.1	6.1	0.63
176	21.8	13.1	8.7	0.60

[a] Units given in 10^{-12} cm^3 s^{-1}, with an estimated uncertainty of ±20%. Measurements were carried out at constant number densities of $N[He] = 6.9 \times 10^{16}$ and $N[C_3H_6] = 1.2 \times 10^{15}$ molecules/cm^3 at all temperatures.

were tested over a wider range, and also showed little effect. At 271 K, while *P*(Pr) changed by a factor of 5, k_2 and the product distribution in the ACT channel increased only slightly. At 245 K, while *P*(Pr) changed by a factor of 7.5, the values of k_2 and the product distribution remained constant within the experimental error. These results agree with our previous limited three-point pressure study in Ar carrier gas that also showed no significant change in k_2 with $P(C_3H_6)$ and with *P*(Ar).[2] The pressure studies therefore indicate second-order or pseudo-second-order kinetics in the measured pressure range, although the overall reaction involves $Bz^{+\bullet}$ and two Pr molecules.

Table 2 and Figure 3 show the temperature dependence of k_2 between 176 and 372 K. The measurements were performed by keeping the number densities constant at $N[He] = 6.9 \times 10^{16}$ and $N[C_3H_6] = 1.2 \times 10^{15}$ molecules/cm^3 throughout the temperature range.

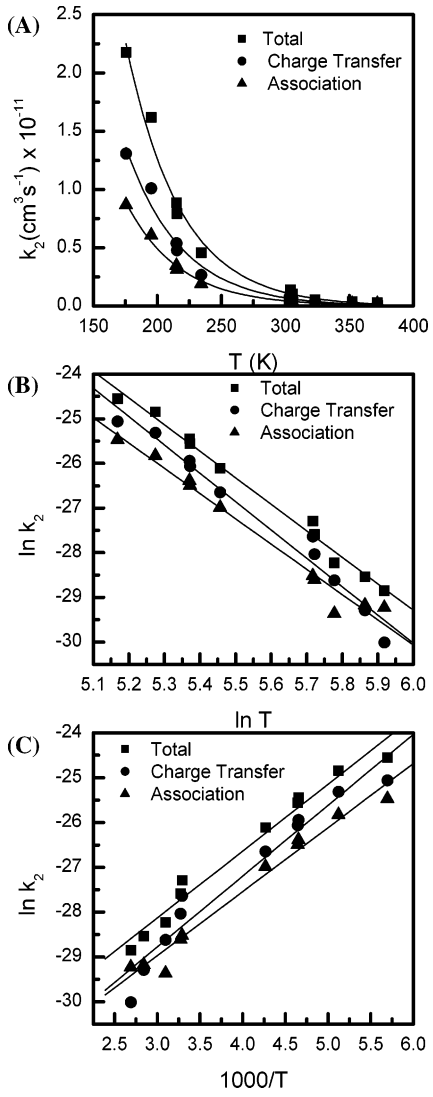

Figure 3. Temperature dependence of the rate coefficients for the overall reaction, the ACT channel to form $C_6H_{12}^{+\bullet}$, and the association channel to form the $(C_6H_6\cdot C_3H_6)^{+\bullet}$ adduct plotted in three functional forms: (A) k_2 vs *T*, (B) ln k_2 vs ln *T*, and (C) ln k_2 vs 1000/*T*. Linear regression correlation coefficients (slope, intercept) and standard deviations (in parentheses) are, for ln k vs 1000/*T*, total reaction: 1.5 (0.1), −32.6 (0.4); ACT: 1.6 (0.1), −33.5 (0.6); association: 1.4 (0.1); −33.2 (0.3). For ln k vs ln T (K), total reaction: −5.9 (0.2), 6.4 (1.2); ACT: −6.4 (0.4), 8.1 (2.2); association: −5.7 (0.3), 3.9 (1.8).

The overall rate coefficient and the rate coefficients into the ACT and association channels increase with decreasing temperature. The results are consistent with our previous observation of a negative temperature coefficient for this reaction in a more limited study using the R2PI−HPMS technique.[2] The product distribution, expressed as the fraction of reaction into the ACT channel, is constant within the temperature range, except for some decrease at the highest temperature; however, where the reactions are slow, the results are subject to error.

For reactions with negative temperature coefficients, the temperature dependence is usually expressed in the Arrhenius form $k = A\exp(-E_a/RT)$ or in a power law form as $k = aT^{-n}$ following Rice−Ramsperger−Kassel−Marcus (RRKM) theory considerations of the complex.[19] In the association reaction $N_2^{+\bullet} + N_2 \rightarrow N_2^{+\bullet}(N_2)$, we showed that the plot of the power law form, rather than the Arrhenius plot of ln *k* versus 1000/*T* was linear over a wide temperature range.[20] Figure 3 shows both

types of plots, that is, ln k_2 versus ln T and ln k_2 versus $10^3/T$, for the overall reaction and the reactions into the ACT and association channels. Both types of plots are linear in the observed range, with some scatter.

The statistics of the plots are shown in the caption of Figure 3. From the slope of ln k_2 versus ln T, we obtain a temperature coefficient of $k_2 = aT^{-5.9}$, while, from ln k_2 versus $1000/T$, we obtain an activation energy of -3.0 kcal/mol. The average value of $k_2 = 2.1 \times 10^{-12}$ cm^3 s^{-1} at 273 ± 2 K from Table 1 yields the functional forms of $k_2 = 496T^{-5.9}$ cm^3 s^{-1} in the exponential form, or $k_2 = 8.58 \times 10^{-15}e^{3000/RT}$ in the Arrhenius form.

Given the negative temperature dependence, the rate coefficient for the overall reaction can reach unit collision efficiency if k_2 assumes the capture collision rate of about 10^{-9} cm^3 s^{-1}. This will occur at 96 K using the power law equation or at 129 K using the Arrhenius equation. Since the product distributions seem to be independent of temperature (Table 2 and Figure 3), the majority of the product (about 60%) will be the ACT condensation product $Pr_2^{+\bullet}$ also at these low temperatures. In other words, below about 100 K, the ACT reaction can approach unit collision efficiency. ACT, maybe from ionized polycyclic aromatics, can therefore be efficient for inducing polymerization at low temperatures, as in planetary atmospheres and interstellar clouds.

3. Temperature and Pressure Effects and the Reaction Mechanism. *(i). Indications of Steric Control*. The slow rate of reaction 1 and its negative temperature coefficient are similar to sterically constrained bimolecular reactions, such as hydride and proton transfer in hindered compounds.[20−24] The role of entropy barriers in these reactions were discussed using transition-state theory (TST).[19,21−24] The double-well model of ion−molecule reactions also relates slow kinetics to constrained transition states.[25,26]

In these models, the initial reaction complex can back-dissociate to reactants through a high-energy, high-density-of-states (high entropy) transition state, or proceed forward through a low-energy, low-density-of-states (low entropy) transition state. In TST terms, the competitive rates of back-dissociation (k_b) or product formation (k_p) are given by $\ln k_p/k_b = (\Delta H^{\ddagger}_b - \Delta H^{\ddagger}_p)/RT - (\Delta S^{\ddagger}_b - \Delta S^{\ddagger}_p)/R$, where the $\Delta H^{\ddagger}$ and $\Delta S^{\ddagger}$ terms correspond to the transition states. At high temperatures, the entropy terms dominate, and, since $\Delta S^{\ddagger}_b \gg \Delta S^{\ddagger}_p$ and $k_b > k_p$, back-dissociation is favored, and the reaction is slow. Conversely, at low temperatures, the enthalpy terms dominate, and, since $\Delta H^{\ddagger}_b \gg \Delta H^{\ddagger}_p$ and $k_p > k_b$, product formation is favored, and the reaction is fast.

Reaction 1 shows these kinetic features, which suggest that the products are formed through low-entropy (low-probability) complexes. In fact, the ab initio calculations below show strict geometrical requirements for activating ACT polymerization in the $Bz^{+\bullet}$(Pr) complex, in other words, a complex with a small conformational entropy. The temperature and pressure studies below are also consistent with this model.

(ii). Temperature Effects. The rate coefficients and their temperature and pressure effects suggest a sequence of steps in the initial stages of the reaction presented in Scheme 1, as discussed below. (For simplicity, the added neutral Pr molecules are omitted on the upper left side of the scheme.)

The magnitude of k_2 is in the range of 10^{-13}−10^{-11} cm^3 s^{-1} in our temperature range. This is slower by 2 to 4 orders of magnitude than the collision rate of about 10^{-9} cm^3 s^{-1}, showing that most of the initial complexes $(Bz^{+\bullet}Pr)^*$ dissociate back to reactants.

Quantitatively, the competition between the forward reaction and back-dissociation of the initial complex $(Bz^{+\bullet}(Pr))^*$ in Scheme 1 leads to eq 2 for k_f, the overall forward rate coefficient.

$$k_f = k_c k_p/(k_b + k_p) \tag{2}$$

Here, k_c is the collision rate coefficient, $k_p = k_{ACT} + k_{assoc}$ is the total rate coefficient of reactions leading to the products, and k_b is the rate coefficient for back-dissociation. Since $k_f \ll k_c$, it follows from eq 2 that $k_p/(k_b + k_p) \ll 1$ and $k_b \gg k_p$, that is, the back-dissociation is much faster than the reaction into the product channels.

The combination of energies and densities-of-states of the transition states (or activation enthalpies and entropies) leads, at high temperatures, to $k_b \gg k_p$, and eq 2 reduces to $k_f = k_c k_p/k_b \ll k_c$, that is, the reaction proceeds with low collision efficiency. In contrast, at low temperatures where $k_b \ll k_p$, eq 2 reduces to $k_f = k_c$, and the reaction becomes faster as it approaches unit collision efficiency. Extrapolating the observed temperature coefficients shows that this transition from slow to fast kinetics will occur below 100 K. In fact, we observed such transitions from slow to fast kinetics in hydride transfer reactions of sterically hindered hydrocarbons and in proton transfer reactions of sterically hindered amines and pyridines.[21−24]

(iii). Pressure Effects. We noted that the kinetics of reaction 1 are similar to sterically constrained bimolecular transfer reactions. However, the present reactions are not bimolecular transfer reactions but association processes where multibody interactions can lead to third-order kinetics. This section will discuss this question and show that the pressure effects support the temperature effects in indicating a rate-controlling step of unimolecular rearrangement through a constrained transition state.

The ACT channel of reaction 1 requires a three-body $Bz^{+\bullet}(Pr)_2$ complex, and association reactions that form adducts such as $Bz^{+\bullet}$(Pr) could often require collisional stabilization by He. If the initial complex $(Bz^{+\bullet}(Pr))^*$ leads directly to these products, then competitive reactions of the complex would yield eqs 3 and 4.

$$k_{f,ACT} = k_c \frac{k_{ACT}[Pr]}{k_{ACT}[Pr] + k_{assoc}[He] + k_b} \tag{3}$$

$$k_{f,assoc} = k_c \frac{k_{assoc}[He]}{k_{ACT}[Pr] + k_{assoc}[He] + k_b} \tag{4}$$

Here, [He] and [Pr] are the number densities of propene and helium. Through eqs 3 and 4, the ACT channel would follow third-order kinetics with respect to Pr, the association reaction would follow third-order kinetics with respect to He, and the ACT/association ratio would be proportional to [Pr] and inversely proportional to [He].

The results in Table 1 do not show these pressure effects. Rather, k_2 and the product ratio vary little with He within experimental error. This is consistent with our previous study[2] in which k_2 was independent of [Ar], and the rate coefficient measured there agrees with the present results within a factor of 2, although Ar is a significantly more efficient third body than He.

The lack of pressure dependence could be consistent with pseudo-second-order association. This could occur by the direct stabilization of the initial $(Bz^{+\bullet}(Pr))^*$ complex under conditions where $k_{assoc}[He] \gg k_{ACT}[Pr] + k_b$ in eq 4, which then reduces to $k_{f,assoc} = k_c$, that is, the association would reach unit efficiency

under these conditions. Similarly, $k_{f,ACT}$ could approach unit efficiency with increasing [Pr]. However, this limiting fast kinetics does not occur under our conditions.

In other words, the reaction does not show the expected pressure effects of three-body reactions where the initial reaction complex $(Bz^{+\bullet}(Pr))^*$ would react directly with He or Pr. Rather, the kinetics are similar to slow bimolecular reactions through constrained transition states.

These considerations suggest that the rate-controlling process in reaction 1 is the unimolecular rearrangement of the initial complex $(Bz^{+\bullet}(Pr))$ through a low-entropy transition state (or competing transition states) to form secondary complexes. One of the secondary complexes, $(Bz^{+\bullet}Pr^{\delta}+)^*$, reacts with Pr to yield the ACT product, while the other complex $(Bz{\cdot}Pr)^{+\bullet *}$ leads to the stable adduct. The unimolecular reactions of the $(Bz^{+\bullet}(Pr))^*$ complex, and therefore the overall rate and the product distribution, are then independent of the partial pressures of He and Pr, as observed here.

The present studies were conducted at [Pr] number densities in the range of $10^{14}-10^{15}$ molecules/cm^3. In our previous study, at lower [Pr] values of $10^{13}-10^{14}$ molecules/cm^3, the ACT/association product ratio increased proportionally with [Pr].[2] In the present work, we noted a similar trend at 370 K, and Table 1 shows a slight effect at 271 K but not at 245 K. It appears that the $(Bz^{+\bullet}Pr^{\delta}+)^*$ ACT complex may rearrange slowly to the $(Bz{\cdot}Pr)^{+\bullet *}$ association complex, especially at higher temperatures, as indicated by the down arrow in Scheme 1. However, competition by collision with Pr eliminates this rearrangement, even at low [Pr] values of about 10^{15} molecules/cm^3.

A further feature of Scheme 1 is that the unimolecular processes corresponding to k_p(ACT) and k_p(assoc) are irreversible. The lack of pressure dependence suggests that these rates are faster than collisions with He, on the order of 10^{-7} sec^{-1} over the observed temperature range. In other words, the initial complex rearranges rapidly to the reactive complexes, which are stabilized by noncollisional mechanisms, as indicated by the lack of pressure effects. Such fast radiative stabilization may be possible in these large complexes with many vibrational degrees of freedom. This mechanism would allow ACT reactions in low-density astrochemical environments.

In summary, the slow rates, negative temperature coefficients, and pressure effects all suggest that the rate-controlling step is the unimolecular rearrangement of the initial complex $[Bz^{+\bullet}(Pr)]^*$ through a constrained transition state or states. The secondary complex $(Bz^{+\bullet}Pr^{\delta}+)^*$ that is formed in this rearrangement reacts with Pr in the ACT channel, and the alternative $(Bz{\cdot}Pr)^{+\bullet *}$ secondary complex leads to the stabilized adduct.

4. Some Analogous Reaction Systems. *(i). $Bz^{+\bullet}$/Ethylene.* In reaction 1, propene is activated for polymerization by partial charge transfer from $Bz^{+\bullet}$, and, similarly, isobutene is activated by charge transfer from toluene$^{+\bullet}$.[1,2] Charge transfer in these systems is possible because the difference between the IEs of the olefins and the core aromatics is small. To explore the limits of reactivity in aromatic ion/olefin systems, we injected $Bz^{+\bullet}$ into ethylene (Et) vapor, where IE(C_2H_4) = 10.5 eV leads to a large difference of 1.3 eV from IE(Bz) = 9.24 eV, and charge transfer in the complex may be too inefficient to initiate condensation. Other than this factor, an ACT reaction similar to reaction 1 could produce a $C_4H_8^{+\bullet}$ ion, for example, 2-butene$^{+\bullet}$ with an exothermicity of 30 ± 1 kcal/mol,[13] similar to the exothermicity of reaction 1. The product could retain the charge since IE(2-butene) = 9.1 eV is lower than that of Bz.

We injected $Bz^{+\bullet}$ into ethylene vapor under various conditions at temperatures from 303 to 197 K. We observed only $Bz^{+\bullet}$ and the $Bz^{+\bullet}$(Et) and $Bz^{+\bullet}$(2Et) adducts but not the dimer $C_4H_8^{+\bullet}$ or its further adducts with Et, as shown in the mass spectra displayed in Figure 4. Condensation similar to reaction 1 was not observed, even at low temperatures where reaction 1 in $Bz^{+\bullet}$/Pr becomes increasingly fast. Another possibility at low temperatures would be that the observed $Bz^{+\bullet}$(2Et) adduct could react with a third Et molecule to yield a $C_6H_{12}^{+\bullet}$ ion. However, this product was also not observed.

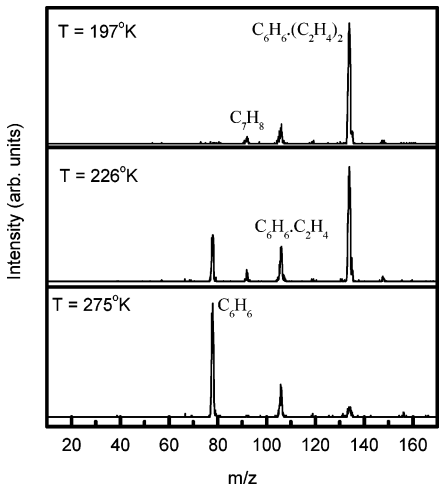

Figure 4. Mass spectra obtained following the injection of $C_6H_6^{\bullet+}$ into 670 mTorr of ethylene in 1.460 Torr of an ethylene/He mixture at a 15 eV (lab.) injection energy at different temperatures. The main ions observed are $Bz^{\bullet+}$ (*m*/*z* 78) and the adducts $Bz^{\bullet+}$(Et) (*m*/*z* 106) and $Bz^{\bullet+}$(2Et) (*m*/*z* 134).

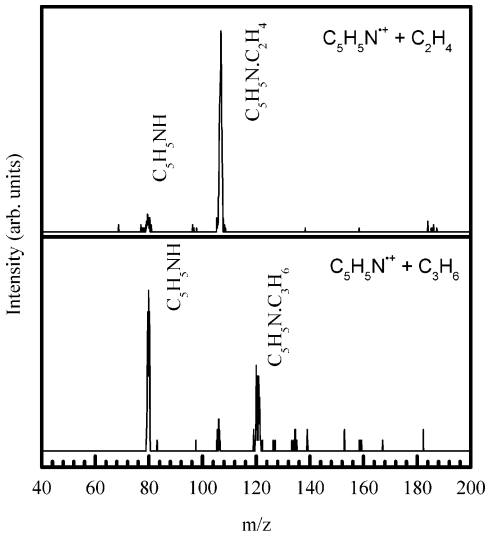

Figure 5. Mass spectra obtained following the injection of pyridine$^{+\bullet}$ into 62 mTorr of ethylene in 2.066 Torr of helium (top panel) and into 300 mTorr of propene in 1.950 Torr of He (bottom panel) at 305 °K and a 15 eV injection energy (lab.).

In summary, although condensation reactions similar to reaction 1 would also be strongly exothermic in $Bz^{+\bullet}$/Et, they are not observed. Apparently, the large IE difference between Bz and Et prevents sufficient partial charge transfer in the complex that could initiate ionic polymerization. This is supported by the ab initio calculations that indicated that most of the charge in the $Bz^{+\bullet}$/Et complex remains on benzene (see below). The absence of an ACT reaction in $Bz^{+\bullet}$/Et therefore supports the importance of intracomplex charge transfer to initiate ion polymerization.

(ii) Pyridine$^{+\bullet}$/Propene. This system is of interest since the IE(Pyridine) = 9.26 eV is nearly identical to the IE(Bz) = 9.24

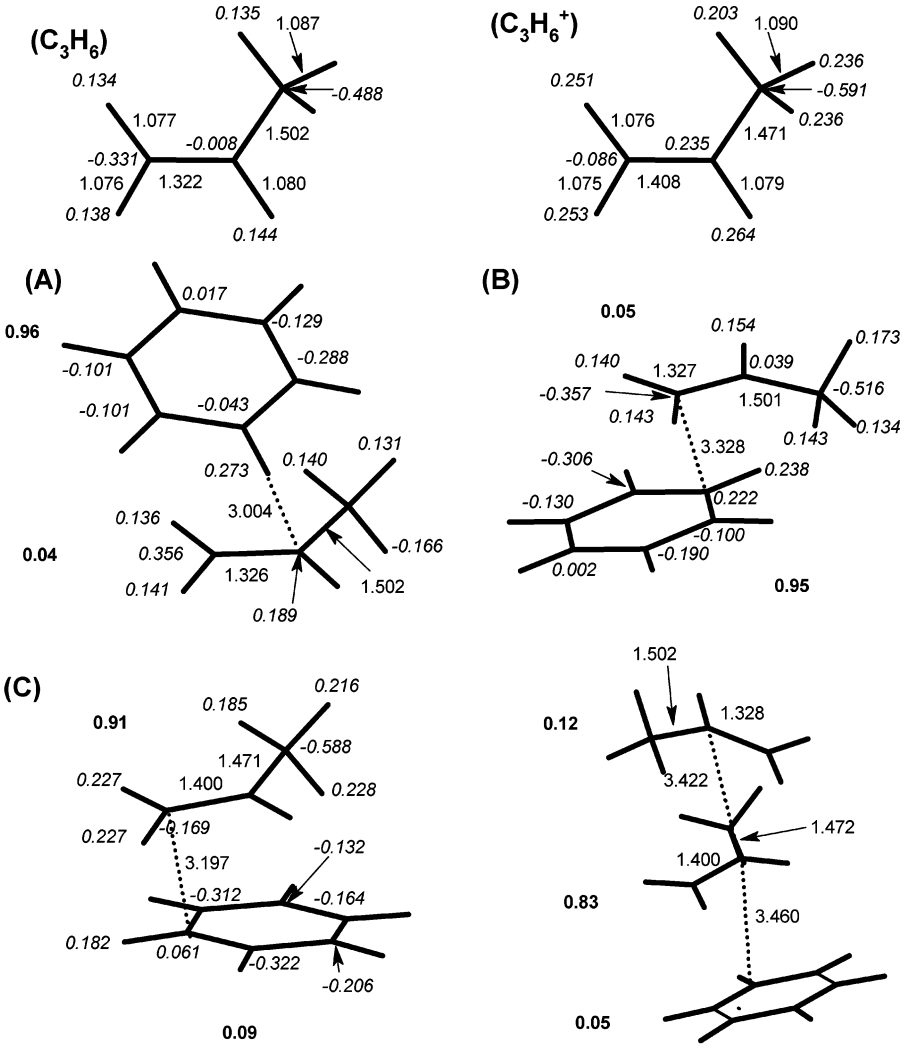

Figure 6. Optimized structures of C_3H_6, $C_3H_6^{+\bullet}$, and $C_6H_6^{+\bullet}(C_3H_6)_{1,2}$ at the ROHF/6-31+G(d,p) level. Bond lengths are given in angstroms; Mulliken atomic charges are in italics, while the charge on each molecule within each cluster is given in bold. The total energies *E*(a.u.), using MP2 energies on ROHF/6-31+G(d,p) geometry and corrected BSSE and ZPE, of C_3H_6, $C_3H_6^{+\bullet}$, $C_6H_6^{+\bullet}$, $C_6H_6^{+\bullet}(C_3H_6)$ (A), $C_6H_6^{+\bullet}(C_3H_6)$ (B), $C_6H_6^{+\bullet}(C_3H_6)$ (C), and $C_6H_6^{+\bullet}(C_3H_6)_2$ are −117.0855708, −116.7824266, −230.4237096, −347.5149617, −347.5149035, −347.5188895, and −464.6122129, respectively. The binding energies (kcal/mol) of C are 3.7 and 14.9, assuming the reactions $C_6H_6^{+\bullet} + C_3H_6 = C_6H_6^{+\bullet}(C_3H_6)$, and $C_6H_6 + C_3H_6^{+\bullet} = (C_6H_6\ (C_3H_6))^{+\bullet}$, respectively. The binding energy of $C_6H_6^{+\bullet}(C_3H_6)_2$ is 5.0 kcal/mol, assuming the reaction $C_6H_6^{+\bullet}(C_3H_6) + C_3H_6 = C_6H_6^{+\bullet}(C_3H_6)_2$.

eV. Therefore, similar to Benzene$^{+\bullet}$, Pyridine$^{+\bullet}$ could also form a Py$^{+\bullet}$(Pr) complex with sufficient charge transfer to initiate polymerization. However, the mass spectrum of this system, displayed in Figure 5, shows that Pyridine$^{+\bullet}$ reacts with C_3H_6 only by H atom transfer to form protonated pyridine $C_5H_5NH^+$ (the H transfer from C_3H_6 to Py$^{+\bullet}$ is exothermic by 33.8 kcal/mol),[13] or to form the adduct Pyridine$^{+\bullet}$(Pr). Apparently, this adduct does not react with Pr to form $C_6H_{12}^{+\bullet}$ since we did not observe this product. Similar results were found for the reaction of Pyridine$^{+\bullet}$ with ethylene, and only protonated pyridine and the Pyridine$^{+\bullet}$(Et) adduct were observed as shown in Figure 5.

In a related study, we observed that Pyridine$^{+\bullet}$ reacts with benzene to form a covalent adduct.[27] It appears that, in Py$^{+\bullet}$(Pr), the propene ligand may be similarly covalently bonded, preventing polymerization with further propene molecules.

5. Computational Results. The structures and charge distributions of the monomers Bz$^{+\bullet}$ and Pr and of the complexes Bz$^{+\bullet}$Pr and Bz$^{+\bullet}$(2Pr) are shown in Figure 6. We may assume that Bz$^{+\bullet}$ induces ionic dimerization by partial charge transfer to Pr and Pr_2 in the complexes. Three isomers with local energy minima were obtained for the $C_6H_6^{+\bullet}(C_3H_6)$ complex, as shown in Figure 6. In isomer A, the propene molecule is located in the plane of the benzene with one of the benzene hydrogens pointing to the center carbon of the propene with a distance of 3.004 Å. In this isomer, 96% of the charge is located on the benzene molecule, while 4% is on the propene. Isomers B and C have the propene molecule above the benzene ring. In isomer B, the propene molecule is partially aligned on top of the benzene ring, whereas, in isomer C, the propene molecule is fully above the benzene ring. The alignment of the propene molecule above the benzene ring has strong correlation with the charge distribution. In isomer B, 95% of the charge is still on the benzene ring, whereas, in isomer C, 91% of the charge is located on the propene molecule.

This specific geometry requirement for internal charge transfer may account for the steric kinetic effects discussed above. The calculations suggest that there may be many accessible conformations of comparable energy, but only conformations in a restricted geometry range can react. The low conformational entropy of the reacting complex leads to the slow rates and negative temperature coefficients, as discussed above.

Charge transfer to propene also affects the geometry of the ligand. Notice the change in the C=C and C−C distances of the propene in isomer C compared to neutral propene. In isomer

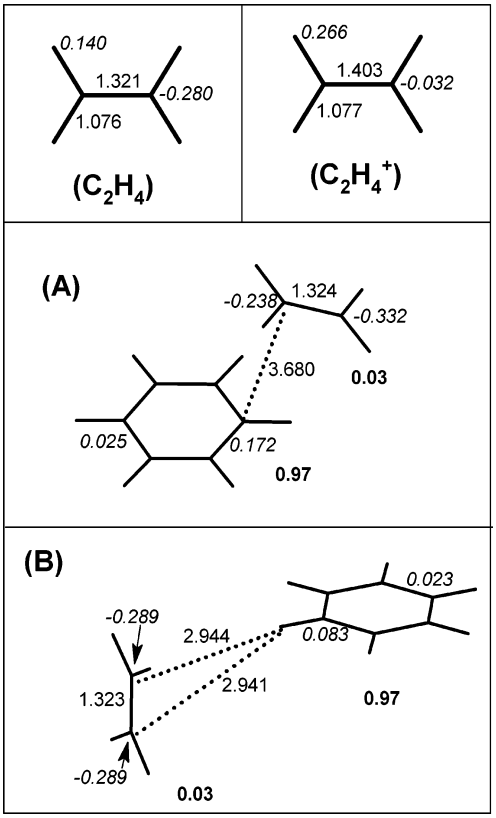

Figure 7. Optimized structures of C_2H_4 and $C_6H_6^+(C_2H_4)$ at the ROHF/6-31+G(d,p) level. Bond lengths are given in angstroms; Mulliken atomic charges are in italics, while the charge on each molecule within each cluster is given in bold. The total energies *E*(a.u.), using MP2 energies on ROHF/6-31+G(d,p) geometry and corrected BSSE and ZPE, of C_2H_4, $C_2H_4^{+\bullet}$, $C_6H_6^{+\bullet}(C_2H_4)$ (A) and $C_6H_6^{+\bullet}(C_2H_4)$ (B) are −78.0430662, −77.71785271, −308.4711608, and −308.4716223, respectively. The binding energies (kcal/mol) of A and B are 3.4 and 3.0, respectively, assuming the reaction $C_6H_6^{+\bullet} + C_2H_4 = C_6H_6^{+\bullet}(C_2H_4)$.

C, the C═C bond is longer (1.400 Å) than that in neutral propene (1.322 Å) but similar to that in the propene cation (1.408 Å). The C−C bond is also shorter (1.471 Å) in isomer C than that in neutral propene (1.502 Å) but is again similar to that in the propene cation (1.471 Å). These changes in the propene geometry reflect the charge transfer from the benzene radical cation to propene. In addition to the differences in charge distributions between the three isomers, isomer C is lower in energy than isomers A and B by 2.5 kcal/mol.

Proceeding to $C_6H_6^{+\bullet}(C_3H_6)_2$, we calculated a structure based on adding a second propene molecule to the low-energy isomer C of the $C_6H_6^{+\bullet}(C_3H_6)$ dimer. Figure 6 shows that some additional charge is transferred to the ligands, and the charge on benzene decreases from 0.09 in $C_6H_6^{+\bullet}(C_3H_6)$ to 0.05 on $C_6H_6^{+\bullet}(C_3H_6)_2$. The first propene bears most of charge (83%) in the complex, while the second propene molecule assumes 12% of the charge. Correspondingly, the geometry of the first propene molecule remains similar to that of the propene cation, while the second propene has a geometry similar to neutral propene. The $Bz^{+\bullet}(Pr)_2$ trimer has a conformation with the terminal olefinic propene groups near each other, which can lead to head-to-head dimerization, forming the $CH_3CH_2CHCHCH_2CH_3^{+\bullet}$ product ion. The corresponding hexene has an IE of 8.83 eV (E conformation) or 8.95 eV (Z conformation),[13] which is lower than the IE of C_6H_6, and therefore it can extract the full charge from the $Bz^{+\bullet}$ core ion.

In the case of ethylene, Figure 7 shows two isomers of the $Bz^{+\bullet}$(Et) adduct. In isomer A, the ethylene molecule is located above the benzene ring, while, in isomer B, the ethylene is located in the plane of the benzene ring and hydrogen-bonded to $Bz^{+\bullet}$ with 90° dihedral angle. In isomer B, the benzene hydrogen is in mid position between the two ethylene carbon atoms. The energy of isomer B is slightly lower (by 0.36 kcal/mol) than that of isomer A.

In contrast to isomer C of the $Bz^{+\bullet}$(Pr), where most of the charge is located on the propene molecule, in $Bz^{+\bullet}$(Et), 97% of the charge remains on the benzene ring. Correspondingly, in $Bz^{+\bullet}$(Pr), efficient charge transfer causes Pr to assume ion-like geometry, whereas, in $Bz^{+\bullet}$(Et), inefficient charge-transfer allows Et to remain similar to neutral ethylene. The difference between charge transfer in $Bz^{+\bullet}$(Pr) and $Bz^{+\bullet}$(Et) parallels the difference in reactivity for ACT condensation and demonstrates the significance of charge transfer in the complex to activate the reaction.

IV. Conclusions

In this paper, we examined the mechanism of a new class of reactions, ACT reactions. We suggested that the reactions are activated by partial charge transfer to the polymerizable ligand in the benzene$^{+\bullet}$(propene) dimer. The present calculations confirmed significant charge transfer in benzene$^{+\bullet}$(propene) but not in benzene$^{+\bullet}$(ethylene). Correspondingly, dimerization is activated with propene but not with ethylene ligands. These observations confirm that the polymerization of the ligand in ACT reactions is activated by partial charge transfer from the core ion.

The reaction proceeds with slow bimolecular kinetics and negative temperature coefficients similar to those of the bimolecular reactions of hindered reagents. The similar kinetics here indicates that the products are formed through a sterically constrained low-entropy (low-density-of-states) transition state. The lack of pressure dependence of the rate constant and of the product distribution and the lack of temperature effects on the product distribution further indicate that the rate is limited by the unimolecular rearrangement of the initial reaction complex, which is subject to steric constraints. The ab initio calculations show that the steric constraints correspond to a specific conformation of the benzene$^{+\bullet}$(propene) that is required for efficient charge transfer in the complex. The low conformational entropy of the reactive complex leads to kinetic effects similar to those in sterically hindered systems.

Extrapolating the negative temperature coefficient suggests that the reaction will change from slow to fast kinetics below 100 K. Fast kinetics at low temperatures suggests that ACT may initiate polymerization in low-temperature astrochemical environments. For example, benzene is present in protoplanetary nebulae,[28] and polycyclic aromatic hydrocarbons (PAHs) are present in interstellar clouds.[15,29] Their ions may initiate the polymerization of unsaturated molecules that condense on the ions. In this manner, ACT reactions of ionized benzene and PAHs can catalyze the formation of complex interstellar molecules.

Acknowledgment. This work was funded by National Science Foundation (CHE-0414613) and NASA (NNG04GH45G) grants. We thank Simon P. Watson for preliminary ab initio calculations of the reaction complexes.

References and Notes

(1) Meot-Ner (Mautner), M.; Pithawalla, Y. B.; Gao, J.; El-Shall, M. S. *J. Am. Chem. Soc.* **1997**, *119*, 8332.

(2) Pithawalla, Y.; Meot-Ner, M.; Gao, J.; El-Shall, M. S.; Baranov, V. I.; Bohme, D. K. *J. Phys. Chem. A* **2001**, *105*, 3908.

(3) Sieck, L. W.; Searles, S. K. *J. Chem.. Phys.* **1970**, *53*, 2601.
(4) Daly, G. M.; Meot-Ner (Mautner), M.; Pithawalla, Y.; El-Shall, M. S. *J. Chem. Phys.* **1996**, *104*, 7965.
(5) Ibrahim, Y.; Alsharaeh, E.; Dias, K.; Meot-Ner (Mautner), M.; El-Shall, M. S. *J. Am. Chem. Soc.* **2004**, *126*, 12766.
(6) Ibrahim, Y. M.; Meot-Ner (Mautner), M.; Alsharaeh, E. H.; El-Shall, M. S.; Scheiner, S. *J. Am. Chem. Soc.* **2005**, *127*, 7053.
(7) Morgan, S.; Castleman, A. W. *J. Am. Chem. Soc.* **1987**, *109*, 2867.
(8) El-Shall, M. S.; Marks, C. *J. Phys. Chem.* **1991**, *95*, 4932.
(9) El-Shall, M. S.; Daly, G. M.; Yu, Z.; Meot-Ner (Mautner), M. *J. Am. Chem. Soc.* **1995**, *117*, 7744.
(10) Zhong, Q.; Poth, L.; Shi, Z.; Ford, J. V.; Castleman, A. W., Jr. *J. Phys. Chem.* **1997**, *101*, 4203.
(11) Shin, D. N.; DeLeon, R. L.; Garvey, J. F. *J. Am. Chem. Soc.* **2000**, *122*, 11887.
(12) Tsunoyama, H.; Ohshimo, K.; Misaizu, F.; Ohno, K. *J. Am. Chem. Soc.* **2001**, *123*, 683.
(13) Hunter, E. P.; Lias, S. G. Proton Affinity Evaluation. Lias, S. G. Ionization Energy Evaluation. In *NIST Chemistry WebBook*, NIST Standard Reference Database Number 69; Linstrom, P. J., Mallard, W. G., Eds.; National Institute of Standards and Technology: Gaithersburg, MD, 2005; http://webbook.nist.gov.
(14) Pithawalla, Y. B.; El-Shall, M. S. In *Solvent-Free Polymerizations and Processes: Minimization of Conventional Organic Solvents*; Long, T. E., Hunt, M. O., Eds.; ACS Symposium Series 713; American Chemical Society: Washington, DC, 1998; pp 232−247.
(15) Allamandola, L. J.; Sandford, S. A.; Wopenka, B. *Science* **1987**, *237*, 56.
(16) Rusyniak, M.; Ibrahim, Y.; Alsharaeh, E.; Meot-Ner, M.; El-Shall, M. S. *J. Phys. Chem. A* **2003**, *107*, 7656.
(17) Rusyniak, M. J.; Ibrahim, Y. M.; Wright, D. L.; Khanna, S. N.; El-Shall, M. S. *J. Am. Chem.* Soc. **2003**, *125*, 12001.
(18) Frisch, M. J.; Trucks, G. W.; Schlegel, H. B.; Scuseria, G. E.; Robb, M. A.; Cheeseman, J. R.; Montgomery, J. A., Jr.; Vreven, T.; Kudin, K. N.; Burant, J. C.; Millam, J. M.; Iyengar, S. S.; Tomasi, T.; Barone, V.; Mennucci, B.; Cossi, M.; Scalmani, G.; Rega, N.; Petersson, G. A.; Nakatsuji, H.; Hada, M.; Ehara, M.; Toyota, K.; Fukuda, R.; Hasegawa, J.; Ishida, M.; Nakajima, T.; Honda, Y.; Kitao, O.; Nakai, H.; Klene, M.; Li, X.; Knox, J. E.; Hratchian, H. P.; Cross, J. B.; Adamo, C.; Jaramillo, J.; Gomperts, R.; Stratmann, R. E.; Yazyev, O.; Austin, A. J.; Cammi, R.; Pomelli, C.; Ochterski, J. W.; Ayala, P. Y.; Morokuma, K.; Voth, G. A.; Salvador, P.; Dannenberg, J. J.; Zakrzewski, V. G.; Dapprich, S.; Daniels, A. D.; Strain, M. C.; Farkas, O.; Malick, D. K.; Rabuck, A. D.; Raghavachari, K.; Foresman, J. B.; Ortiz, J. V.; Cui, Q.; Baboul, A. G.; Clifford, S.; Cioslowski, J.; Stefanov, B. B.; Liu, G.; Liashenko, A.; Piskorz, P.; Komaromi, I.; Martin, R. L.; Fox, J.; Keith, T.; Al-Laham, M. A.; Peng, C. Y.; Nanayakkara, A.; Challacombe, M.; Gill, P. M. W.; Johnson, B.; Chen, W.; Wong, M. W.; Gonzalez, C.; Pople, J. A. *Gaussian 03*, revision C.02; Gaussian, Inc.: Wallingford, CT, 2004.
(19) Meot-Ner (Mautner), M., In *Ion−Molecule Reactions*; Bowers, M. T., Ed.; Academic Press: New York, 1979; Vol. 1, pp 198−268.
(20) Meot-Ner, M.; Field, F. H. *J. Chem. Phys.* **1974**, *61*, 3742.
(21) Meot-Ner (Mautner), M.; Solomon, J. J.; Field, F. H.; Gershinowitz, H. *J. Phys. Chem.* **1974**, *78*, 1733.
(22) Meot-Ner (Mautner), M.; Field, F. H. *J. Am. Chem. Soc.* **1978**, *100*, 1356.
(23) Meot-Ner (Mautner), M.; Smith, S. C. *J. Am. Chem. Soc.* **1991**, *113*, 862.
(24) Meot-Ner (Mautner), M.; Sieck, L. W.; El-Shall, M. S.; Daly, G. M. *J. Am. Chem. Soc.* **1995**, *117*, 7737.
(25) Olmstead, W. N.; Brauman, J. I. *J. Am. Chem. Soc.* **1977**, *99*, 4219.
(26) Olmstead, W. N.; Brauman, J. I. *J. Mass Spectrom.* **1995**, *30*, 1653.
(27) Ibrahim, Y. M.; Watson, S. P.; Rusyniak, M.; Meot-Ner (Mautner), M.; El-Shall, M. S. To be submitted for publication.
(28) Cernicharo, J.; Heas, A. M.; Tielen, A. G. G. M.; Pardo, J. R.; Herpin. F.; Guelin, M.; Waters, L. B. F. M. *Astrophys. J.* **2001**, *546*, L123.
(29) Bernstein, M. P.; Sandford, S. A.; Allamandola, L. J.; Gillette, J. S.; Clemett, S. J.; Zare, R. N. *Science* **1999**, *283*, 1135.